INTERNATIONAL JOURNAL OF NUMERICAL MODELLING: ELECTRONIC NETWORKS, DEVICES AND FIELDS
Int. J. Numer. Model. 2002; **15**:371–383 (DOI: 10.1002/jnm.459)

Accuracy of the frequency-domain TLM method and its application to microwave circuits

J. Hesselbarth*,† and R. Vahldieck

Laboratory for Electromagnetic Fields, and Microwave Electronics (IFH), Swiss Federal Institute of Technology (ETH), Gloriastrasse 35, CH-8092 Zurich, Switzerland

SUMMARY

This paper investigates the accuracy and convergence of frequency-domain (FD) TLM solutions and describes a method to identify non-physical solutions. The numerical dispersion characteristics of various discretization schemes ('nodes') are compared. The occurrence of non-physical solutions when solving three-dimensional problems is discussed and a method to identify the non-physical solutions is described. The accuracy of the FDTLM method is shown to be of second order as long as singularities are absent, whereas it is between first and second order if the computational domain includes field singularities.

KEY WORDS: TLM; frequency domain; dispersion; spurious solutions; convergence

1. INTRODUCTION

The idea of the transmission line matrix (TLM) method dates back to the 1940s, when Kron [1,2] described how a waveguide cavity was modelled by a transmission line network, which was actually built and voltages were physically measured, allowing to conclude about the electromagnetic fields in the original problem. This approach fell into oblivion until digital computers became widely available [3,4]. With the development of the so-called symmetrical condensed node (SCN) in 1987 [5], TLM became relevant for practitioners. The principles of the frequency-domain TLM (FDTLM) method were published first in 1992 [6,7]. Another frequency-domain approach is the so-called method of minimal autonomous blocks (MAB). This method is similar to a large extend to the FDTLM method, except that the transmission line equivalence is not used. It employs an original notation and the TLM similarity was never mentioned in the literature [8,9].

Various discretization schemes ('nodes') have been developed for time-domain TLM [10] as well as for frequency-domain TLM [6,7,11–13]. In the present paper, the accuracy, or numerical dispersion, of the FDTLM nodes will be compared and the respective worst case errors will be partly presented in analytical form, thus making a comparison easy and clear.

*Correspondence to: Jan Hesselbarth, Laboratory for Electromagnetic Fields, and Microwave Electronics (IFH), Swiss Federal Institute of Technology (ETH), Gloriastrasse 35, CH-8092 Zurich, Switzerland.
†E-mail: jhesselb@ifh.ee.ethz.ch

Published online 29 May 2002
Received 1 June 2001
Revised 1 December 2001

Another problem which has been reported for time-domain TLM is the occurrence of spurious solutions. It will be shown below, that non-physical solutions also occur in FDTLM solutions, namely for cavity resonances and waveguide eigensolutions. A method is presented which allows to find out whether a solution is actually physical or not.

Finally, the present paper will show that the FDTLM solution accuracy indeed converges with second order, as long as the computational domain does not include singularities. If it does, the accuracy will degrade to first order, depending on the problem.

2. DERIVATION OF NODE SCATTERING MATRICES

Various discretization schemes of Maxwell's equations following the approach of the SNM [5] have been developed in the past for both TLM and FDTLM. A conclusive derivation of the different node scattering matrices starts with obtaining the constitutive equations of any TLM node from power conservation laws [14], keeping time synchronism if necessary and enforcing Maxwell's equations. The latter is based on a mapping between field components and link-line voltage waves, followed by central differencing of the field components [10]. In a frequency domain formulation of TLM, stubs are avoided, and time synchronism between voltage waves travelling in different directions is not necessary. Thus, FDTLM has degrees of freedom to define the impedances and propagation constants on the link-lines. This choice differs for the various proposed schemes, such as the following:

- The characteristic admittance node (CAN) sets all link-line impedances equal to the impedance of the medium and derives the link-line propagation constants accordingly [6,7].
- The propagation constant node (PCN) sets all link-line propagation constants equal to half the propagation constant of a plane wave in the medium and derives the link-line impedances accordingly [11,12].
- The finite difference node (FDN) avoids link-lines completely, resulting in a discretization scheme similar to those of the finite difference frequency-domain method [13].

As a result, the node scattering matrix of the SCN of size 12×12 is obtained, which relates the vector of incident voltages, (V^{inc}), and the vector of reflected voltages, (V^{ref}), as

$$(V^{\mathrm{ref}}) = [S] \cdot (V^{\mathrm{inc}}) \tag{1}$$

For a practical problem, many SCN are combined in a block-diagonal matrix $[S]$, and the voltage vectors are simply concatenated.

3. PLANE WAVE DISPERSION

If a plane-wave propagates through a homogeneous medium which is modelled with a mesh of nodes, the numerical wavenumber k_{num} will usually differ from the physical wavenumber k, a phenomenon described as *numerical dispersion*. If the medium is modelled using a periodic mesh of nodes, then only one mesh cell must be taken into consideration. In the following, the

numerical dispersion characteristics of the three aforementioned discretization schemes (CAN, PCN, FDN) are evaluated.

The numerical dispersion characteristics of the CAN scheme were analysed previously [15,16]. However, these investigations were limited to plane-wave propagation in loss-free medium and in the yz-plane of the co-ordinate system only.

In the following, the homogeneous medium is considered to be isotropic and characterized by its (complex) permittivity and permeability. The plane wave is characterized by the wavenumber and the direction of propagation. All field components are known at the boundaries of the node cell. By using the mapping between the fields of the plane wave and the voltage waves of the SCN at the node boundaries, a matrix $[T]$ can be found such that

$$(V^{\text{inc}}) = [T] \cdot (V^{\text{ref}}) \tag{2}$$

Hereby, the matrix $[T]$ depends on the wavenumber k of the plane wave. The vectors of incident and reflected voltages have to respect both Equations (1) and (2) at the same time. This is only possible if the node scattering matrix $[S]$ in Equation (1) uses a wavenumber k_{num} which differs slightly from k. The numerical wavenumber k_{num} is found from

$$\det\{[S] \cdot [T] - [U]\} = 0 \tag{3}$$

with the unit matrix $[U]$. The numerical dispersion error can be equated as

$$\text{error} = \left| \frac{k - k_{\text{num}}}{k} \right| \cdot 100\% \tag{4}$$

3.1. Cubic node shape and loss-free material

For cubic node shape (cube size Δx), CAN and PCN, are identical and show zero error in axis direction and the maximum error in the direction of the space diagonal ($\varphi = 45^\circ$, $\theta = 54.7^\circ$ in spherical co-ordinates). The analytical solution for the worst case error is found as

$$k_{\text{num}}\Delta x = \arccos\left(\frac{1}{4} + \frac{3}{4}\cos\left(\frac{2}{\sqrt{3}}k\Delta x\right)\right) \tag{5}$$

For small node cells, this simplifies to

$$k_{\text{num}}\Delta x = k\Delta x\left(1 - \frac{1}{72}(k\Delta x)^2\right) \tag{6}$$

The finite difference node FDN shows minimum error in space diagonal direction and maximum error in axis direction (this behaviour is common for FDTD schemes). The analytical solutions for the dispersion error of cubic FDN is found as

$$k_{\text{num}}\Delta x = 2\left(k\Delta x - \sqrt{q}\tan\left(\frac{k\Delta x}{2\sqrt{q}}\right)\right) \tag{7}$$

for plane-wave propagation in axis direction ($q = 1$), co-ordinate plane diagonal direction ($q = 2$), and space diagonal direction ($q = 3$), respectively. This simplifies for small node cells to

$$k_{\text{num}}\Delta x = k\Delta x\left(1 - \frac{1}{12q}(k\Delta x)^2\right) \tag{8}$$

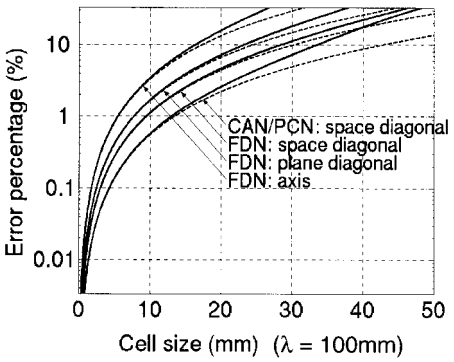

Figure 1. Numerical dispersion error for CAN/PCN and FDN for cubic node geometry of variable size up to $\lambda/2$ ($f = 3$ GHz, air, $\lambda_0 = 100$ mm). Solid lines: exact analytical formulas. Dashed lines: approximate formulas for small node cells.

Table I. Numerical dispersion error ranges for different discretization schemes (CAN, PCN, FDN) for different node aspect ratios (node volume kept constant) modelling plane-wave propagation in loss-less medium.

	CAN (%)	PCN (%)	FDN (%)
Δx: Δy: $\Delta z = 1:1:1$, $\Delta z = \lambda/20$	0–0.14		0.28–0.83
Δx: Δy: $\Delta z = 1:1:2$, $\Delta z = \lambda/12.6$	0–0.79	0–0.19	0.23–2.13
Δx: Δy: $\Delta z = 1:2:4$, $\Delta z = \lambda/10$	0.23–5.47	0–0.35	0.16–3.43

Note that the worst case error for CAN and PCN is only about half the best error of FDN and about one-sixth of the worst case error of FDN. Figure 1 shows this behaviour as a function of the node cell size.

3.2. *Non-cubic node shape and loss-free material*

The accuracy of the discretization schemes decreases as the node cell shape deviates from the cubic form. The error distribution shows a strong dependence on the direction of the incident plane wave, and as a general rule, the worst case errors grow strongly. Note that the nodes CAN and PCN produce now different results. Furthermore, CAN is dispersionless for propagation in co-ordinate axis direction as long as the node cell cross-section perpendicular to this axis is square. In general, the PCN produces much smaller errors than CAN and FDN. This is illustrated by Table I, showing the dispersion error ranges for nodes of different aspect ratio, keeping the node volume constant.

3.3. *Cubic node shape and lossy material*

A plane wave propagating through an homogeneous, lossy medium (permittivity ε_r, conductivity σ) will be affected both in phase and magnitude by errors introduced by the numerical scheme. These errors will add to the errors due to node cell shape and size.

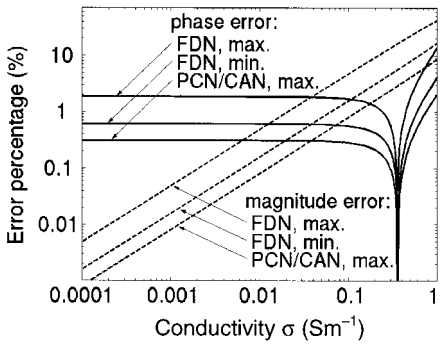

Figure 2. Numerical dispersion error for CAN/PCN and FDN for a cubic node of $\Delta x = 5$ mm, $\varepsilon_r = 2.2$, $f = 3$ GHz. Solid lines: phase error. Dashed lines: magnitude error over a distance of $\lambda = 67.4$ mm. Note that the minimum magnitude and phase errors for PCN/CAN are zero (in axis direction).

Consider the following illustrative case: a cubic node cell of size 5 mm, filled with a material having $\varepsilon_r = 2.2$, at $f = 3$ GHz. As before, FDN shows the smallest error in space diagonal direction and the worst-case error in axis direction. PCN and CAN are identical, having no error in axis direction and the worst case error in space diagonal direction. Figure 2 shows the error ranges in function of the conductivity of the material. As it was the case for the loss-free material, the error in magnitude of FDN is about 2–6 times larger than the worst case error of PCN and CAN. Furthermore, the error in magnitude of the wavenumber k is very small for commonly used low-loss dielectric materials, but it grows approximately with a power law and becomes significant for larger conductivity ($\sigma > \approx 0.1$ S/m is common for, e.g. many biological materials). The phase error is almost unaffected by a small conductivity. However, it shows an interesting zero at higher conductivity. At this point, the plane wave propagates without phase error through the mesh in any direction. The dispersion zero occurs at a conductivity given approximately by $\sigma \approx \omega\ \varepsilon_0\ \varepsilon_r$. This equation holds exactly as if $\Delta x \to 0$.

4. MATRIX ALGORITHMS FOR MICROWAVE CIRCUIT PROBLEMS

In the following, matrix algorithms are briefly presented for the treatment of problems appearing during the analysis of microwave circuit structures, such as resonance frequencies of a cavity resonator, cut-off frequencies and eigenmodes of a waveguide, and scattering parameters of a three-dimensional structure. The appearance of spurious solutions and the convergence behaviour of these algorithms will be discussed in subsequent paragraphs.

4.1. Cavity resonance frequency

The scattering matrices of all nodes of the computational domain can be put together in a block-diagonal matrix [S], each row and column of which containing between 4 and 6 non-zero complex entries. Then, Equation (1) holds for the entire computational domain. The connection between the link-lines of all nodes of the computational domain as well as the connection to

boundaries can be described with a very sparse connection matrix $[C]$ as

$$(V^{\text{inc}}) = [C] \cdot (V^{\text{ref}}) \tag{9}$$

For a resonator at resonance, Equations (1) and (9) are combined to give

$$\text{Det}\{[U] - [S] \cdot [C]\} = \text{Det}\{[S] - [C]^{-1}\} = 0 \tag{10}$$

where $[U]$ denotes the unit matrix. The search of a singularity in Equation (10) while varying the frequency is rather involved if $[S]$ is large. By simply calculating the determinant for various frequencies, a very small frequency step may become necessary in order to prevent missing a root. Alternatively, the singularity can also be found by searching a zero of the smallest singular value. The so-called singular value decomposition (SVD) of a matrix is computationally more expensive than the calculation of the determinant, but the frequency-dependence of the smallest singular values is rather nice and allows for the application of efficient root-searching algorithms.

4.2. Waveguide mode cut-off frequency

The calculation of the cut-off frequency of a mode in a waveguide is a resonance problem [17]. Hereby, the waveguide is considered to be homogeneous in propagation direction. At cut-off, the wave resonates in the transverse plane. Thus, the computational domain can be a one node thick transverse slice. At cut-off, all modes degenerate to be either of type TE (no electric field in waveguide direction) or TM (no magnetic field in waveguide direction). For the case of TE-cut-off, a magnetic wall boundary condition limits the computational domain in the transverse planes, whereas for the case of TE-cut-off, perfect electric conductor boundary conditions are applied. The cut-off frequencies are then given by Equation (10) and are found using a zero search algorithm.

4.3. Waveguide mode propagation constant

In order to find eigensolutions (propagation constant, field distribution) of waveguides at a given frequency, periodic boundary conditions (Floquet conditions) are enforced onto a one node thick transverse slice. The scattering matrix of the computational domain is then converted into an ABCD matrix (works best *via* scattering transfer matrix $[T]$), from which the eigensolutions are found [7,8]. This procedure includes two inversions of square matrices of size $4N_{\text{node}}$, one inversion of a matrix of size $2N_{\text{node}}$, and the solution of a standard eigenvalue problem involving a matrix of size $2N_{\text{node}}$ (N_{node} is the number of SCN in the computational domain).

4.4. Scattering parameters of three-dimensional structures

Given a three-dimensional microwave circuit with port boundaries connected to semi-infinite waveguides, the analysis of this structure can be divided into three steps: (i) calculation of the eigenmodes of the waveguides at the ports, (ii) calculation of the field distribution inside the computational domain and (iii) expansion of the field distributions at the port planes in terms of waveguide eigenmodes and derivation of scattering parameters. The second step is computationally the most expensive as it involves the decomposition of a large, sparse matrix composed of all node scattering matrices. Instead, the computational domain can be divided in subdomains, which will result in several inversions of small, dense matrices instead. Note that

the algorithm allows the connected waveguides being outside the computational domain, and higher order modes as well as evanescent modes are automatically taken into account by the eigenmode expansion of the waveguide described above [7].

5. NON-PHYSICAL SOLUTIONS

Spurious or non-physical solutions appear in TLM solutions due to the fact that the electromagnetic fields are sampled twice in space, or, in other words, the underlying mapping between fields and link line voltage waves results in an equation system which is overdetermined by a factor of two. This problem can be overcome by special measures such as the ATLM scheme [18]. The occurrence and treatment of non-physical solutions in FDTLM is discussed below.

5.1. Non-physical resonance modes

For a given physical resonance mode, Equation (10) yields two singularities. These two solutions are usually slightly different from each other as a result of numerical dispersion. They can, however, also occur at the same frequency giving rise to a double root in Equation (11). In order to determine which singularity actually corresponds to a physically meaningful resonance mode, the field distributions and thus the eigenvectors have to be calculated, e.g. from

$$\{[U] - [S] \cdot [C]\}(V^{\text{ref}}) = 0, \text{ (frequency at the singularity)} \tag{11}$$

The electromagnetic fields are then readily calculated from (V^{ref}).

The test whether the fields are physically meaningful is done locally, that is, for each node separately. For a simple test, the field components, which are known from (V^{inc}) and (V^{ref}) at the boundary of a SCN, must be transformed to the node centre by applying the propagation constants of the respective link-lines. Then, each field component is related to two pairs of complex values in the node centre. For example, E_x is given by the voltages on the y-directed, x-polarized link-lines (this gives one pair of complex values in the node centre) and by the voltages on the z-directed, x-polarized link-lines (this gives the second pair). For a physical field solution, the phases of a given pair of values are always identical, whereas for a non-physical solution, they usually differ by 180°.

An additional difficulty arises if the resonance frequencies of physical and non-physical solutions are (almost) identical. Then, none of the two eigenvectors gives a meaningful field distribution. However, there exists always a linear superposition of the two eigenvectors which does represent a physical solution. The weighting coefficient of the superposition is found by enforcing (in one node) the phases of the corresponding voltages to be equal. In the frame of numerical accuracy, all field components of all nodes will give the same weighting factor. The superposed field is a physical solution as it can be verified by the test described above.

As resonators can have physically degenerate resonances (two or more different resonance modes having the same resonance frequency), the numerical solution can give twice as many degenerate eigensolutions. Again, a suitable superposition of all these eigenvectors gives the correct number of orthogonal, physical eigensolutions. In general, however, physically degenerated resonances will have numerically distinct resonance frequencies if a graded mesh is used, because of the numerical anisotropy introduced by the graded mesh.

Table II. Fundamental resonance frequencies of a cubic resonator obtained by a graded mesh and the distinction between physical and non-physical solutions.

Resonance frequency (MHz)	Error in frequency (%)	Physical solution or not?
4978.5	−6.1	Non-physical
5049.5	−4.7	Non-physical
5127.5	−3.2	Non-physical
5222.74	−1.4	Physical, $E_x = E_y = 0$
5224.02	−1.4	Physical, $E_x = E_z = 0$
5224.93	−1.4	Physical, $E_y = E_z = 0$

To give an example, consider a cubic cavity resonator of size $(40\ \text{mm})^3$ which is meshed with $4 \times 4 \times 4$ nodes. This cavity has a three-fold physical resonance at 5.30 GHz. By using cubic nodes of identical shape, a six-fold singularity is found at $f = 5.23$ GHz. If a graded mesh is used, however, the singularities will appear at slightly different frequencies because of the numerical anisotropy introduced by the graded mesh. Suppose the following node dimensions

- in x-direction: 8.5 mm, 9.5 mm, 10.5 mm, 11.5 mm,
- in y-direction: 7.75 mm, 9.25 mm, 10.75 mm, 12.25 mm,
- in z-direction: 7 mm, 9 mm, 11 mm, 13 mm.

A frequency sweep yields six distinct singularities around 5.3 GHz as shown in Table II. The eigensolutions are tested for physical relevance using the phase-test described above. Note that in this case, the physical solutions have three non-zero field components only. The phase-test should be applied to non-zero field components only.

5.2. *Non-physical eigensolutions*

The waveguide eigenmode algorithm described above results in physical as well as non-physical solutions. Both classes of solutions can be propagating (carrying real power) as well as evanescent (carrying imaginary power). It is therefore important to know how to recognize a non-physical mode and to find out whether non-physical modes affect the solution of three-dimensional scattering parameter problems.

Consider the rectangular waveguide cross-section shown in Figure 3, discretized with four identical cubic SCN (CAN/PCN). A magnetic wall symmetry plane can be applied. Although the cut-off frequencies of the TE_{n0} modes are calculated exactly (no dispersion in x-axis direction), at other frequencies but cut-off, numerical dispersion will result in an error in the propagation constants.

Having two nodes (and a magnetic wall symmetry plane) in the computational domain, the two-dimensional eigenvalue problem results in the following four eigenvalues (propagation constants)

$$\gamma_{\text{I}} = \alpha_{\text{I}} + j\beta_{\text{I}} = \frac{1}{\Delta}\operatorname{arcosh}(3 + 2\sqrt{2} + 2(\sqrt{2} + 2)\cos(\Delta k_0)) \tag{12}$$

$$\gamma_{\text{II}} = \alpha_{\text{II}} + j\beta_{\text{II}} = \frac{1}{\Delta}\operatorname{arcosh}(3 - 2\sqrt{2} - 2(\sqrt{2} - 2)\cos(\Delta k_0)) \tag{13}$$

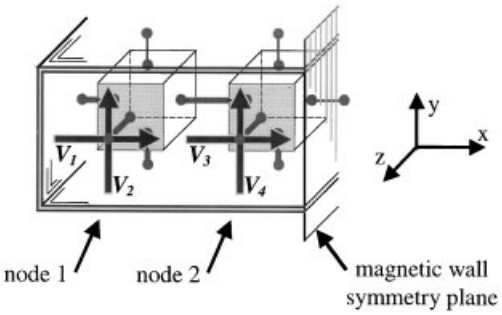

Figure 3. Rectangular waveguide cross section discretized with two FDTLM nodes (symmetry applied).

$$\gamma_{\mathrm{III}} = \alpha_{\mathrm{III}} + j\beta_{\mathrm{III}} = \frac{1}{\Delta}\operatorname{arcosh}(-3 + 2\sqrt{2} + 2(\sqrt{2} - 2)\cos(\Delta k_0)) \tag{14}$$

$$\gamma_{\mathrm{IV}} = \alpha_{\mathrm{IV}} + j\beta_{\mathrm{IV}} = \frac{1}{\Delta}\operatorname{arcosh}(-3 - 2\sqrt{2} - 2(\sqrt{2} + 2)\cos(\Delta k_0)) \tag{15}$$

where Δ denotes the node dimension, and the eigenvectors (of the form $(v) = \{(V_1), (V_2), (V_3), (V_4)\}$, see Figure 3)

$$(v_{\mathrm{I}}) = \{(0), (-1 - \sqrt{2}), (0), (1)\} \tag{16}$$

$$(v_{\mathrm{II}}) = \{(0), (\sqrt{2} - 1), (0), (1)\} \tag{17}$$

$$(v_{\mathrm{III}}) = \{(1 - \sqrt{2}), (0), (1), (0)\} \tag{18}$$

$$(v_{\mathrm{IV}}) = \{(1 + \sqrt{2}), (0), (1), (0)\} \tag{19}$$

Because the total link-line voltages (which are elements of the eigenvectors) are proportional to the transverse electric field components of the respective polarizations, (v_{I}) and (v_{II}) are found to describe the exact field magnitudes of the TE_{30} and TE_{10} modes, respectively, whereas (v_{III}) and (v_{IV}) are found to represent non-physical solutions.

When considering the properties of the arcosh(...) function as in Equations (12)–(15), it is found that an evanescent mode solution corresponds to $\cosh(\gamma\Delta) > 1$, cut-off occurs at $\cosh(\gamma\Delta) = 1$, a propagating mode solution has $+1 > \cosh(\gamma\Delta) > -1$, and solutions with $\cosh(\gamma\Delta) \leqslant -1$ are non-physical. Thus, propagating solutions may be either physical or non-physical. To become clear, Figure 4 shows α and β over normalized frequency. Note that a maximum frequency is given as $f_{\max} = c/2\Delta$, where all propagating modes have the same wavenumber of $\beta = \pi/\Delta$. Here, the node dimension equals half a wavelength. At reasonably low frequencies (approx. $f < c/4\Delta$), the non-physical propagating mode (III) is faster than the speed of light and can be crossed out. For inhomogeneous waveguides involving dielectrics, this frequency limit lowers. The propagation modes, either physical and non-physical, carry real power. Experience shows, however, that the scattering between them is zero (within numerical limits), that is, a three-dimensional structure does not couple between physical and non-physical fields.

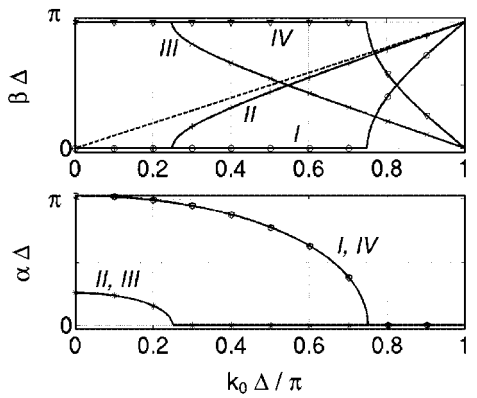

Figure 4. Phase constant β (top) and attenuation constant α (bottom) of the four eigensolutions (Equations (12)–(15)) as a function of normalized frequency. The dashed line describes the wavenumber of a plane wave in free space.

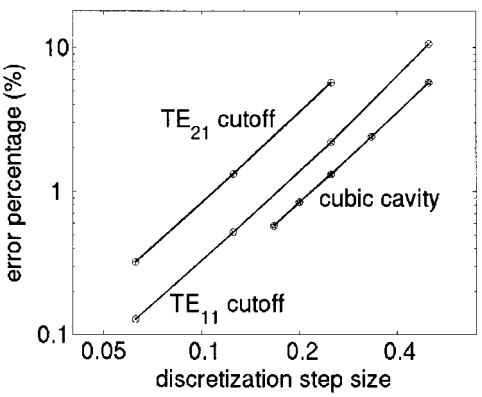

Figure 5. Quadratic increase of the accuracy versus mesh density shown for cubic resonator TE_{110} resonance (2^3, 3^3, 4^3, 5^3, and 6^3 cubic nodes, respectively) and rectangular waveguide TE_{11} and TE_{21} cut-offs (2×1, 4×2, 8×4, and 16×8 cubic nodes, respectively).

6. ACCURACY AND CONVERGENCE OF THE SOLUTIONS

By keeping the node aspect ratios in a mesh constant and increasing the resolution of the mesh, the accuracy of the FDTLM solution will be enhanced. The increase of the accuracy is of second order for propagating waves and of first order for evanescent fields. Two examples will illustrate this.

Consider a cavity resonance problem, for example, a cubic cavity and the cut-off frequencies of a rectangular waveguide (without the use of symmetry planes). Figure 5 shows the decrease of error with decrease of mesh period for the fundamental cavity resonance as well as TE_{11} and TE_{21} mode cut-off frequencies. A division of the mesh period by two results in an error magnitude divided by four, showing clearly second order accuracy.

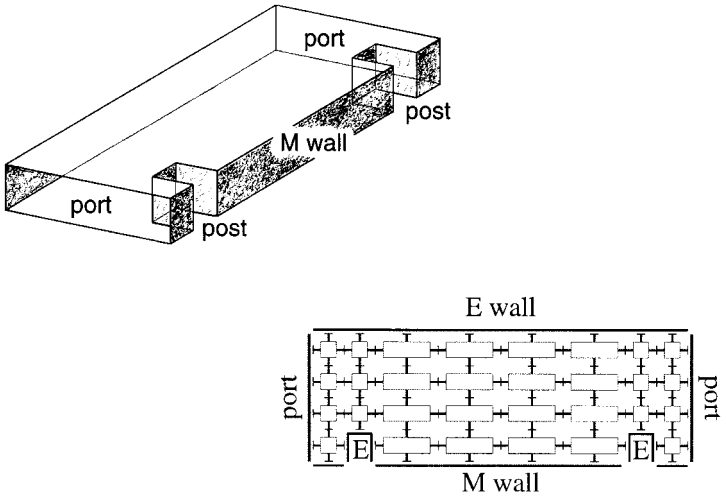

Figure 6. Left: Drawing of the single resonator waveguide filter. Right: Rough mesh of 30 FDTLM nodes (waveguide width 2 mm × 11.43 mm, overall length 33.43 mm, cavity length 22 mm, post 5.715 mm × 2.8575 mm).

Consider next a double-post waveguide resonator band-pass filter as shown in Figure 6. This structure shows both propagating wave sections (the cavity) and evanescent field sections (the vicinity of the post wedges). An accurate reference solution was obtained using a mode-matching approach (pass-band frequency 9136 MHz). A very rough FDTLM mesh of 30 nodes (Figure 6, right) is found to result in an frequency error of -1.50%. Dividing the node size by two gives an error of -0.54%, an additional node size reduction by a factor of two results in -0.20% error of the frequency. Thus, this structure shows an increase of accuracy of order 1.45 when refining the mesh period. This is consistent with the observation reported in Reference [19], showing an accuracy increase of only first order in the vicinity of a metallic fin.

7. CONCLUSION

The numerical dispersion of various FDTLM nodes has been evaluated and compared, in part analytically, for both cubic and non-cubic nodes, in loss-free and lossy media. The so-called propagation constant node [11,12] was found to show superior accuracy compared to other nodes.

Non-physical solutions have been found in the analysis of resonators and waveguides. It was shown how these solutions can be identified.

The accuracy of the resonance frequency of a cavity without field singularities was found to increase with second order. However, a waveguide filter response was found to converge only by an order of 1.45, which was due to the field singularities in the computational domain.

REFERENCES

1. Kron G. Equivalent circuits to represent the electromagnetic field equations. *Physical Review* 1943; **64**:126–128.
2. Whinnery JR, Concordia C, Ridgway W, Kron G. Network analyzer studies of electromagnetic cavity resonators. *Proceedings of the IRE* 1944; **32**:360–367.
3. Johns PB, Beurle RL. Numerical solution of 2-dimensional scattering problems using a transmission-line matrix. *Proceedings of the IEE* 1971; **118**:1203–1208.
4. Hoefer WJR. The transmission line matrix (TLM) method. *Numerical Techniques for Passive Microwave and Millimeter-Wave Structures*, Chapter 8, Itoh T. (ed.). Wiley: New York, 1989; 486–591.
5. Johns PB. A symmetrical condensed node for the TLM method. *IEEE Transactions on Microwave Theory Techniques* 1987; **35**:370–377.
6. Johns DP, Wlodarczyk AJ, Mallik A, Christopoulos C. New TLM technique for steady-state field solutions in three dimensions. *Electronics Letters* 1992; **28**:1692–1694.
7. Jin H, Vahldieck R. The frequency-domain transmission line matrix method—A new concept. *IEEE Transactions on Microwave Theory Techniques* 1992; **40**:2207–2218.
8. Nikolskij VV, Nikolskaja TI. *Decomposition technique in tasks of electrodynamics (Декомпозиционный Подход к Задачам Электродинамики)* Nauka: Moscow, 1983 (in Russian).
9. Machac J. Analysis of discontinuities in waveguiding structures by MAB method. *IEE Proceedings-H* 1992; **139**:351–357.
10. Trenkic V, Christopoulos C, Benson TM. Development of a general symmetrical condensed node for the TLM method. *IEEE Transactions on Microwave Theory Techniques* 1996; **44**:2129–2135.
11. Berini P, Wu K. A new frequency domain symmetrical condensed TLM node. *IEEE Microwave Guided Wave Letters* 1994; **4**:180–182.
12. Johns DP. Improved node for frequency-domain TLM: The 'distributed node'. *Electronics Letters* 1994; **30**:500–502.
13. Jin H, Vahldieck R. A new frequency-domain TLM symmetrical condensed node derived directly from Maxwell's equations. *Proceedings of the IEEE MTT Symposium*, New York, 1995; 487–490.
14. AI-Mukhtar DA, Sitch JE. Transmission-line matrix method with irregularly graded space. *IEE Proceedings-H* 1981; **128**:299–305.
15. Johns DP, Christopoulos C. Dispersion characteristics of 3-D frequency-domain TLM. *Electronics Letters* 1993; **29**:1536–1537.
16. Johns DP, Christopoulos C. Dispersion of time-domain and frequency-domain formulations of the symmetrical condensed TLM node. *Proceedings of the Second International Conference on Computation in Electromagnetics.* IEE Publication number 384, London, April 1994; 295–298.
17. Hesselbarth J, Vahldieck R. Mesh grading and cutoff frequencies in the frequency-domain TLM method. *Proceedings of the IEEE MTT Symposium*, New York, 1998; 1551–1554.
18. Russer P, Bader B. The alternating transmission line matrix (ATLM) scheme. *Proceedings of the IEEE MTT Symposium*, New York, 1995; 19–22.
19. Simons NRS, Siushansian R, LoVetri J, Cuhaci M. Comparison of the transmission-line matrix and finite-difference time-domain methods for a problem containing a sharp metal edge. *IEEE Transactions on Microwave Theory Techniques* 1999; **47**:2042–2045.

AUTHORS' BIOGRAPHIES

Jan Hesselbarth received the Dipl-Ing degree in electrical engineering from Dresden University of Technology (TU), Dresden, Germany, in 1995. He then joined the Sensor Systems division of EADS, Ulm, Germany, as a design engineer. Since 1997 he is with the Swiss Federal Institute of Technology, Zurich, Switzerland. His research interests focus on modelling methods for passive microwave circuits.

Rüdiger Vahldieck received the Dipl-Ing and the Dr-Ing degrees in electrical engineering from the University of Bremen, Germany, in 1980 and 1983, respectively. From 1984 to 1986 he was a Research Associate at the University of Ottawa, Canada. In 1986 he joined the Department of Electrical and Computer Engineering at the University of Victoria, British Columbia, Canada where he became a Full Professor in 1991. During fall and spring 1992–93 he was a visiting scientist at the 'Ferdinand-Braun-Institut für-Hochfrequenztechnik' in Berlin, Germany. He is now Professor for field theory at the Swiss Federal Institute of Technology, Zürich, Switzerland. His research interests include numerical methods to model electromagnetic fields for computer-aided design of microwave, millimeter wave and opto-electronic

integrated circuits. He is also interested in system simulation and design of broadband fiber-optic communication systems and subsystems. Dr Vahldieck, together with three co-authors, received the outstanding publication award of the Institution of Electronic and Radio Engineers in 1983. He is a Fellow of the IEEE and has published more than 200 technical papers mainly in the field of microwave CAD. He is on the editorial board of the IEEE Transaction on Microwave Theory and Techniques, serves as Associate Editor of the IEEE. Microwave and Wireless Components Letters and is on the Technical Program Committee of the IEEE International Microwave Symposium.

射 频 和 天 线 设 计 培 训 课 程 推 荐

易迪拓培训(www.edatop.com)由数名来自于研发第一线的资深工程师发起成立，致力并专注于微波、射频、天线设计研发人才的培养；我们于 2006 年整合合并微波 EDA 网(www.mweda.com)，现已发展成为国内最大的微波射频和天线设计人才培养基地，成功推出多套微波射频以及天线设计经典培训课程和 ADS、HFSS 等专业软件使用培训课程，广受客户好评；并先后与人民邮电出版社、电子工业出版社合作出版了多本专业图书，帮助数万名工程师提升了专业技术能力。客户遍布中兴通讯、研通高频、埃威航电、国人通信等多家国内知名公司，以及台湾工业技术研究院、永业科技、全一电子等多家台湾地区企业。

易迪拓培训课程列表：http://www.edatop.com/peixun/rfe/129.html

射频工程师养成培训课程套装

该套装精选了射频专业基础培训课程、射频仿真设计培训课程和射频电路测量培训课程三个类别共 30 门视频培训课程和 3 本图书教材；旨在引领学员全面学习一个射频工程师需要熟悉、理解和掌握的专业知识和研发设计能力。通过套装的学习，能够让学员完全达到和胜任一个合格的射频工程师的要求…

课程网址：http://www.edatop.com/peixun/rfe/110.html

ADS 学习培训课程套装

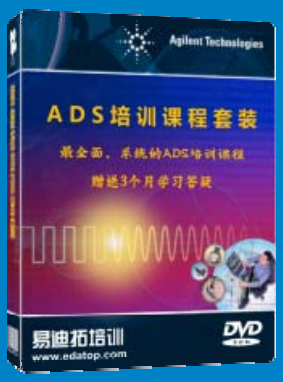

该套装是迄今国内最全面、最权威的 ADS 培训教程，共包含 10 门 ADS 学习培训课程。课程是由具有多年 ADS 使用经验的微波射频与通信系统设计领域资深专家讲解，并多结合设计实例，由浅入深、详细而又全面地讲解了 ADS 在微波射频电路设计、通信系统设计和电磁仿真设计方面的内容。能让您在最短的时间内学会使用 ADS，迅速提升个人技术能力，把 ADS 真正应用到实际研发工作中去，成为 ADS 设计专家...

课程网址： http://www.edatop.com/peixun/ads/13.html

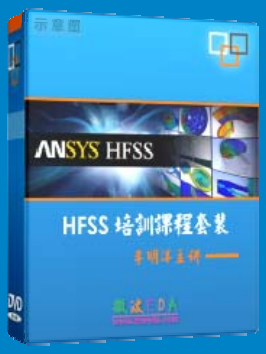

HFSS 学习培训课程套装

该套课程套装包含了本站全部 HFSS 培训课程，是迄今国内最全面、最专业的 HFSS 培训教程套装，可以帮助您从零开始，全面深入学习 HFSS 的各项功能和在多个方面的工程应用。购买套装，更可超值赠送 3 个月免费学习答疑，随时解答您学习过程中遇到的棘手问题，让您的 HFSS 学习更加轻松顺畅…

课程网址：http://www.edatop.com/peixun/hfss/11.html

CST 学习培训课程套装

该培训套装由易迪拓培训联合微波 EDA 网共同推出，是最全面、系统、专业的 CST 微波工作室培训课程套装，所有课程都由经验丰富的专家授课，视频教学，可以帮助您从零开始，全面系统地学习 CST 微波工作的各项功能及其在微波射频、天线设计等领域的设计应用。且购买该套装，还可超值赠送 3 个月免费学习答疑…

课程网址：http://www.edatop.com/peixun/cst/24.html

HFSS 天线设计培训课程套装

套装包含 6 门视频课程和 1 本图书，课程从基础讲起，内容由浅入深，理论介绍和实际操作讲解相结合，全面系统的讲解了 HFSS 天线设计的全过程。是国内最全面、最专业的 HFSS 天线设计课程，可以帮助您快速学习掌握如何使用 HFSS 设计天线，让天线设计不再难…

课程网址：http://www.edatop.com/peixun/hfss/122.html

13.56MHz NFC/RFID 线圈天线设计培训课程套装

套装包含 4 门视频培训课程，培训将 13.56MHz 线圈天线设计原理和仿真设计实践相结合，全面系统地讲解了 13.56MHz 线圈天线的工作原理、设计方法、设计考量以及使用 HFSS 和 CST 仿真分析线圈天线的具体操作，同时还介绍了 13.56MHz 线圈天线匹配电路的设计和调试。通过该套课程的学习，可以帮助您快速学习掌握 13.56MHz 线圈天线及其匹配电路的原理、设计和调试…

详情浏览：http://www.edatop.com/peixun/antenna/116.html

我们的课程优势：

※ 成立于 2004 年，10 多年丰富的行业经验，

※ 一直致力并专注于微波射频和天线设计工程师的培养，更了解该行业对人才的要求

※ 经验丰富的一线资深工程师讲授，结合实际工程案例，直观、实用、易学

联系我们：

※ 易迪拓培训官网：http://www.edatop.com

※ 微波 EDA 网：http://www.mweda.com

※ 官方淘宝店：http://shop36920890.taobao.com